ЖЭТФ, 2013, том 144, вып. 4 (10), стр. 859–866

ELECTRON MOMENTUM DENSITY, BAND STRUCTURE, AND STRUCTURAL PROPERTIES OF SrS

G. Sharma[a*], **N. Munjal**[b], **V. Vyas**[b], **R. Kumar**[c], **B. K. Sharma**[c], **K. B. Johsi**[d,e]

[a] *Department of Pure & Applied Physics, University of Kota 324010, Kota, India*

[b] *Department of Physics, Banasthali University 304022, Banasthali, India*

[c] *Department of Physics, University of Rajasthan 302004, Jaipur, India*

[d] *Department of Physics, MLS University 313002, Udaipur, India*

[e] *Department of Physics & Astronomical Sciences, Central University of Himachal Pradesh 176215, Dharamshala, India*

Received April 6, 2013

The electron momentum density, the electronic band structure, and the structural properties of SrS are presented in this paper. The isotropic Compton profile, anisotropies in the directional Compton profiles, the electronic band structure and density of states are calculated using the *ab initio* periodic linear combination of atomic orbitals method with the CRYSTAL06 code. Structural parameters of SrS — lattice constants and bulk moduli in the B1 and B2 phases — are computed together with the transition pressure. The computed parameters are well in agreement with earlier investigations. To compare the calculated isotropic Compton profile, measurement on polycrystalline SrS is performed using 5Ci-^{241}Am Compton spectrometer. Additionally, charge transfer is studied by means of the Compton profiles computed from the ionic model. The nature of bonding in the isovalent SrS and SrO compounds is compared on the basis of equal-valence-electron-density profiles and the bonding in SrS is found to be more covalent than in SrO.

DOI: 10.7868/S0044451013100179

1. INTRODUCTION

Strontium sulfide (SrS), a II–VI compound, has been studied experimentally as well as theoretically [1–16] owing to technological applications in luminescent, magneto-optical, and infrared-sensitive devices [2, 15]. Under normal conditions, it crystallizes in the rock-salt (B1) structure and shows a structural phase transition to the cesium chloride (B2) structure under pressure. A number of investigations on SrS are devoted to studying the phase transition, optical and electronic properties, etc. (see, e. g., [1–16]).

The Compton profile, $J(p_z)$, is an important observable to characterize the momentum density distribution of electrons in solids [17, 18]. The $J(p_z)$ is defined as

$$J(p_z) = \int_{-\infty}^{\infty}\int_{-\infty}^{\infty} \rho(p_x, p_y, p_z)\, dp_x dp_y, \qquad (1)$$

where $\rho(p_x, p_y, p_z)$ is the electron momentum density in solids [17]. It gives the projection of the electron momentum density along the scattering vector direction (z-axis). It is one of the few observables that can be both calculated and directly measured. It enables unfolding Fermi surface calipers in metals and related systems, nature of bonding, bond length and charge transfer in compounds and alloys [17, 18]. Despite extensive investigations, neither theoretical nor experimental attempt has been made to explore the electron momentum density and thereby the Compton profile in SrS.

*E-mail: gsphysics@gmail.com

In this work, therefore, a systematic theoretical and experimental Compton profile study of SrS is carried out. The ionic model is applied to examine the charge transfer in SrS by means of Compton profiles. Other electronic properties — the electronic band structure and density of states — are also presented. Moreover, the structural properties such as equilibrium lattice constants and bulk moduli are computed for the B1 and B2 phases together with the transition pressure for the B1→B2 structural transition. All theoretical calculations are performed using the periodic linear combination of the atomic orbitals (LCAO) method implementing the CRYSTAL06 code. To compare the calculated Compton profile, a measurement on the polycrystalline sample of SrS has been done with a 5Ci-Compton spectrometer based on the ^{241}Am radioisotope.

The paper is organized as follows. In Sec. 2, a brief description of the experiment is given. The computational details are presented in Sec. 3. In Sec. 4, we present and discuss the results, and conclusions are given in Sec. 5.

2. EXPERIMENTAL DETAILS

The Compton profile measurement on a polycrystalline sample of SrS was carried out using a 5Ci-^{241}Am gamma-ray spectrometer. The spectrometer offers a modest resolution (Gaussian, full width at half maximum) around 0.6 a.u. The salient features of the experimental setup are available elsewhere [19]. In the present measurement, the incident gamma rays of 59.54 keV were scattered at an angle $166^\circ \pm 3.0^\circ$ by the sample (pellet of 18 mm diameter, 3.2 mm thickness, and 1.627 gm/cm^3 effective density). The scattered radiation was recorded using an HPGe detector (Canberra model, GL0110S) and associated electronics to collect 45000 counts at the Compton peak. To achieve the true Compton profile, the raw data were corrected for several systematic corrections such as the background, instrumental resolution, sample absorption, scattering cross section and multiple scattering, etc. [20, 21]. Finally, the corrected profile was normalized on the corresponding free atom [22] area, i. e., 24.049 electrons within the momentum range 0–7 a.u. The 1s electrons of Sr were neglected since they do not contribute to the experimental Compton profile within 0–7 a.u. in the current setup.

3. COMPUTATIONAL DETAILS

3.1. DFT-LCAO method

The structural and electronic properties of SrS were computed using the *ab initio* LCAO method embodied in the CRYSTAL code [23]. In this method, the crystalline orbitals $\psi_i(\mathbf{r}, \mathbf{k})$ are linear combination of Bloch functions $\varphi_\mu(\mathbf{r}, \mathbf{k})$ defined in terms of local functions $\varphi_\mu(\mathbf{r})$, normally referred as atomic orbitals. The Gaussian basis sets were taken for Sr and S [24]. The exchange and correlation are treated under the generalized gradient approximation. The correlation functional proposed by Perdew, Burke, and Ernzerhof (PBE) [25], which has been one of the reasonably successful correlation functionals [26–28], is used, while exchange is considered by applying Becke's ansatz [29]. The self-consistent calculations were performed considering 145**k** points in the irreducible Brillouin zone with tight tolerances and the self-consistency was achieved within 10 cycles.

3.2. Ionic model

The ionic-model-based theoretical Compton profiles of SrS for various charge transfer configurations were determined by using the free atom profiles [22] of Sr and S. The valence profiles for various $Sr^{+x}S^{-x}$ ($0.0 \le x \le 2.0$) configurations were derived by transferring x electron from the $5s$ shell of Sr to the $3p$ shell of S, and then these profiles were added to the core contributions to obtain the total ionic profiles. All these ionic profiles were then appropriately normalized to compare with the experimental data.

4. RESULTS AND DISCUSSION

In the present study, we have computed directional and spherically averaged Compton profiles of SrS. In practice, calculations are not directly compared with the experimental data. Rather, these are convoluted by the residual instrumental function or a Gaussian function to include resolution effects, and thereafter the convoluted data are used for comparison. Generally, the convolution smears the calculated Compton profiles. The experimental and unconvoluted spherically averaged theoretical (DFT-LCAO) Compton profiles of SrS are given in Table 1. The ionic profiles based on the charge transfer configurations $Sr^{+x}S^{-x}$ with $0.0 \le x \le 2.0$ in step of 0.5 are also given in the table. These data may be useful for comparison with experiment and calculations that may appear in future.

Study of anisotropies facilitates examining the directional features in the electron momentum density. The anisotropies in Compton profiles are therefore derived from the directional Compton profiles computed along the [100], [110], and [111] principal crystallographic directions. The [100]–[110], [100]–[111], and

Table 1. The experimental and unconvoluted theoretical Compton profiles of polycrystalline SrS. Experimental errors ($\pm\sigma$) are also shown at a few points. All profiles are normalized to 24.049 electrons within the range 0 to +7 a.u.

$J(p_z)$, e/a.u.						
p_z	DFT-PBE	Ionic				Experiment
		$x = 0.5$	$x = 1$	$x = 1.5$	$x = 2.0$	
0.00	12.067	14.403	13.649	12.896	12.142	11.965 ± 0.034
0.10	12.040	13.892	13.298	12.704	12.110	11.935
0.20	11.853	12.690	12.435	12.179	11.923	11.759
0.30	11.425	11.390	11.414	11.439	11.463	11.431
0.40	11.071	10.565	10.724	10.884	11.043	10.992
0.50	10.479	9.795	9.984	10.173	10.362	10.487
0.60	9.776	9.078	9.250	9.423	9.595	9.927
0.70	8.995	8.358	8.501	8.643	8.786	9.299
0.80	8.171	7.649	7.763	7.876	7.990	8.618
1.00	6.587	6.355	6.424	6.493	6.563	7.273 ± 0.026
1.20	5.384	5.337	5.379	5.420	5.462	6.069
1.40	4.581	4.590	4.614	4.638	4.662	5.044
1.60	4.046	4.060	4.073	4.087	4.100	4.307
1.80	3.681	3.684	3.691	3.698	3.706	3.766
2.00	3.415	3.410	3.414	3.418	3.422	3.392 ± 0.017
3.00	2.533	2.533	2.534	2.536	2.537	2.304 ± 0.013
4.00	1.816	1.815	1.816	1.818	1.819	1.647 ± 0.011
5.00	1.266	1.265	1.266	1.267	1.268	1.206 ± 0.009
6.00	0.901	0.902	0.902	0.903	0.904	0.915 ± 0.008
7.00	0.660	0.661	0.662	0.662	0.662	0.686 ± 0.007

[110]–[111] anisotropies are plotted in Fig. 1. In order to expect magnitude of experimental anisotropy, the three plotted DFT-LCAO anisotropies are derived from the convoluted directional Compton profiles. The anisotropies in the Compton profiles remain within $\sim$ 2 a.u. Thereafter, a major contribution comes from the core electrons that have identical contributions in all directions, and hence the anisotropies vanish. The figure shows that the [110]–[111] anisotropy has the smallest magnitude in the entire range. The anisotropies [100]–[110] and [100]–[111] show a similar trend at all momenta. The maximum anisotropy can be seen between the [100] and [111] directions. It indicates a larger role of the [100] direction compared to the other two with regard to the momentum density distribution in SrS. Consequently, specific features — extremes in anisotropies — are anticipated at $2\pi/a = 0.55$, 1.1 a.u. The extremes in anisotropies related to the [100] direction can be clearly seen at these positions in Fig. 1. As expected, these features appear at a lower momentum in the [110]–[111] anisotropy. Moreover, the positive nature of all these anisotropies around $p_z = 0$ indicates larger occupied states along the [100] direction with low momentum. To quantify these directional features, the directional Compton profile measurements on SrS would be valuable.

We next compare the Compton profile calculations with our own measurement. First, we compare Compton profiles computed from various ionic arrangements. The difference (convoluted ionic-experiment) profiles are shown in Fig. 2. A similar approach was used to estimate the charge transfer in other compounds [30–32]. It is clear from the figure that the effect of variation of the charge on Sr and S is visible only up to 1.5 a.u. All ionic arrangements show an identical trend in the high-momentum region. To esti-

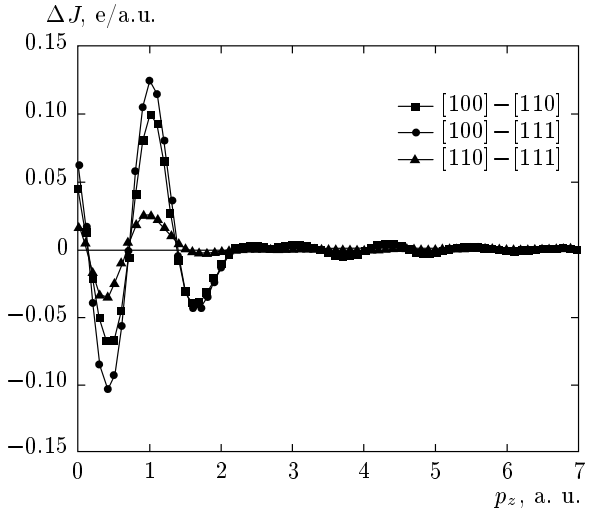

Fig. 1. Directional anisotropies $\Delta J(p_z)$ in SrS for the direction pairs [100]–[110], [100]–[111], and [110]–[111]. All anisotropies are obtained from convoluted DFT-LCAO Compton profiles

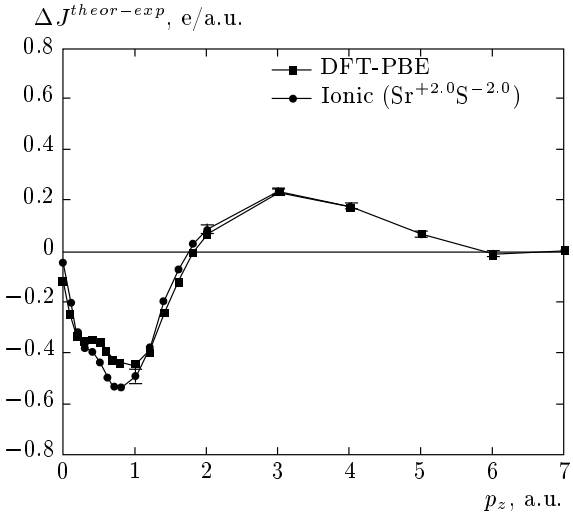

Fig. 3. Difference between the convoluted theoretical (DFT-LCAO and best agreed ionic) and the experimental Compton profiles of SrS. Experimental errors ($\pm\sigma$) are also shown at some points

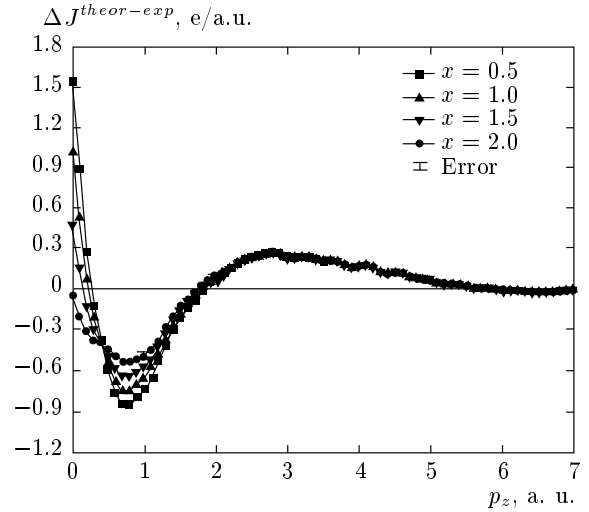

Fig. 2. Difference between convoluted ionic Compton profiles and the experimental Compton profile of SrS. Experimental errors ($\pm\sigma$) are also shown at some points

mate the charge transfer, we have computed χ^2 and observed that the $Sr^{+2.0}S^{-2.0}$ configuration gives the best agreement with the measurement. Therefore, the ionic model suggests transfer of 2.0 electrons from Sr to S. Second, we compare the Compton profile computed from the DFT-LCAO method. The difference profiles $\Delta J = J^{theor}(p_z) - J^{exp}(p_z)$ derived from the convoluted DFT-LCAO method and the best agreed ionic arrangement with the experiment ($Sr^{+2.0}S^{-2.0}$) are plotted in Fig. 3. The figure reveals that the difference curves derived from both schemes show differences in the low-momentum region $0.0 \le p_z \le 2.0$. It may be due to the inclusion of solid state effects in the DFT-LCAO method because this is a highly sensitive region where valence electrons contribute largely to the electron momentum density. The maximum differences shown by the DFT-LCAO and ionic model with the experimental $J(0)$ value are about 3.76 % and 4.52 % respectively. The overall agreement, examined on the basis of χ^2, is shown by the DFT-LCAO model with the measurement. Beyond 2.0 a.u., difference curves derived from both schemes overlap each other. This is well expected because the contribution of core electrons, which are less affected by solid formation, dominates in this region. In the high-momentum region 3–7 a.u., the differences are beyond the experimental error. This is probably due to the pellet nonuniform thickness, which gives rise to a nonuniform absorption correction. Because this correction is isotropic in nature, it naturally cancels when anisotropies are measured.

We now examine the nature of bonding in isostructural and isovalent SrS and SrO compounds. For this, we compute equal valence electron density (EVED) profiles on the p_z/p_F scale, where p_F is the Fermi momentum, from the experimental and theoretical Compton profiles of valence electrons of SrS and SrO. The experimental valence profiles are deduced by subtract-

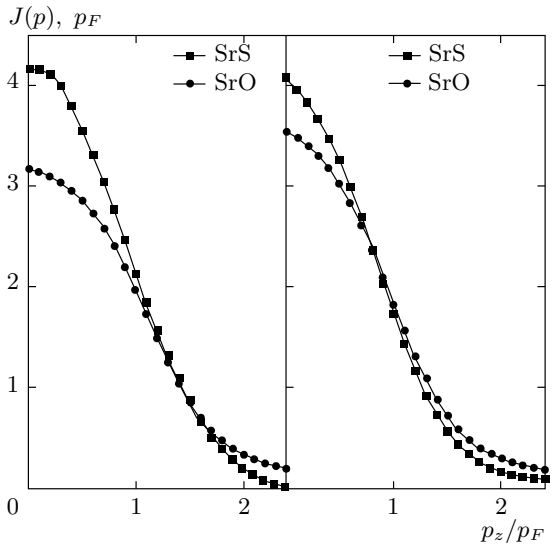

Fig. 4. The EVED profiles of SrS and SrO. The left and right panels respectively show the EVED profiles derived from the experimental and convoluted theoretical (DFT-LCAO) valence profiles

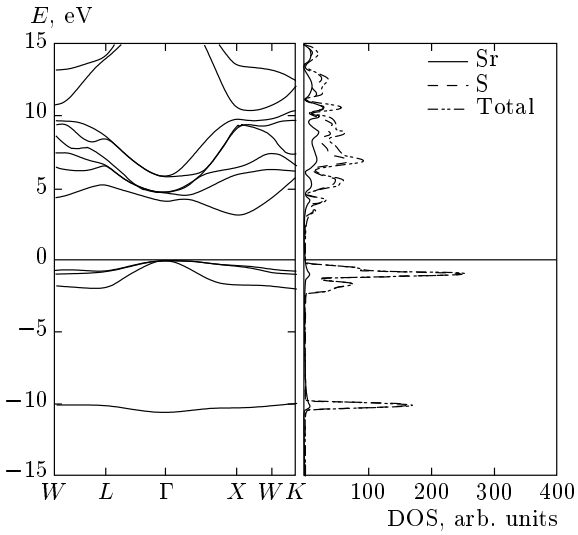

Fig. 5. Energy band structure of the B1 phase of SrS

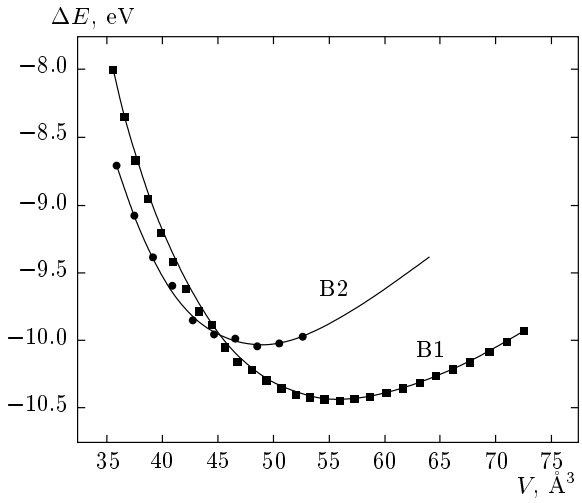

Fig. 6. First-principle $E(V)$ curves for B1 and B2 structures of SrS obtained from DFT-LCAO calculations. The scattered points show calculated energies and the solid lines show the fitted $E(V)$ curves according to the Birch–Murnaghan equation of state

ing the convoluted core from total experimental profiles. These valence electron profiles are normalized to 4.0 electrons and multiplied by the corresponding Fermi momentum ($p_F = 0.862, 1.006$ a.u. for SrS and SrO respectively). The EVED profile scheme provides a way to understand the nature of bonding in isostructural and isovalent compounds [33, 34]. The experimental EVED profiles of the two compounds are plotted in the left panel of Fig. 4. For SrO, data is taken from our own earlier measurement [35]. In the right panel, we show the EVED profiles derived from the DFT-LCAO scheme for the two compounds. It is clear from the figure that the EVED profile of SrS is higher than that of SrO at lower values of p_z/p_F. This indicates the larger covalent and smaller ionic character of SrS compared to SrO. This is well supported by Fig. 3, where the complete ionic model deviates from the experiment more than the DFT-LCAO scheme does. The less ionic character of SrS compared to SrO is well supported by the ionicity factors f_i proposed by Phillips [36].

The electronic band structure and density of states (DOS) for the B1 phase of SrS are plotted in Fig. 5. In Table 2, we give our energy bandgaps, calculated at the principal symmetry points, along with the experimental and theoretical data available in the literature. It is clear from Table 2 that the present PBE–GGA electronic band gaps are in good agreement with experiment. From the calculated DOS for SrS, as shown in Fig. 5, we find that below and above the Fermi level, the electronic states of sulphur dominate the density of states.

To determine the structural parameters, the total energies are calculated for rocksalt (B1) and cesium chloride (B2) phases of SrS at different volumes around the equilibrium primitive cell volume V_0. The plots of calculated total energies versus volume for SrS in both structures are given in Fig. 6. The fitted $E(V)$ curves accoding to Birch–Murnaghan equations of state (EOS) [28, 37] are represented by solid lines in the figure. It shows that the energy of the lowest point of

Table 2. Band gaps (eV) for the B1 phase SrS

		Γ–Γ	X–X	L–L	Γ–X	Γ–L
Present work		4.004	3.438	6.087	3.016	5.214
Experimental	[8]	5.387	–	–	4.32	–
Other Calculations	FP-LAPW [9]	–	–	6.357	2.536	–
	LDA [10]	3.65	–	–	2.10	–
	GGA-PBE [10]	3.80	–	–	2.15	–
	GGA(WC) [10]	3.60	–	–	2.30	–
	[11]	3.51	–	–	–	–
	GGA [4]	3.88	3.06	6.60	2.60	5.46
	[13]	–	–	–	2.30	–
	[14]	–	–	7.017	2.326	–
	FP-LAPW [5]	3.74	2.90	6.38	2.45	5.36
	LMTO-LDA [6]	3.58	2.85	7.39	2.56	6.12
	[14]	–	–	–	3.70	–
	HF [15]	6.83	8.88	10.03	7.50	8.52
	LAPW-LDA [16]	3.51	2.78	5.0	2.30	2.58

Table 3. The lattice constants a_0, bulk moduli B_0, and their pressure derivatives B_0' for SrS in the B1 and B2 structures together with the B1-to-B2 transition pressure P_t

		Present work	Experimental	Other calculations
B1	a_0, Å	6.074	6.024 [1]	6.05 [2], 6.035 [3], 6.024 [4], 6.076 [5], 5.774 [6]
	B_0, GPa	50.5	58 [1]	48 [3], 53.9 [4], 47 [5], 62 [6]
	B_0'	3.9553		3.96 [3], 4.66 [4], 4.19 [5]
	P_t, GPa	18.77	18 [1]	17.7 [2], 18 [5], 17.1 [6], 17.5 [7]
B2	a, E	3.65	3.61 [1]	3.65 [2], 3.655 [3], 3.646 [4], 3.68 [5], 3.481 [6]
	B_0, GPa	73.284		50.71 [2], 51 [3], 50.6 [4], 50 [5], 67.3 [6]
	B_0'	4.6		3.99 [2], 4.38 [3], 4.50 [4], 3.88 [5]

the B1 structure is below that of the B2 structure. We have computed the equilibrium lattice constant a_0, the bulk modulus B_0, and its pressure derivatives B_0' for B1 and B2 phases of SrS by fitting the Birch–Murnaghan EOS [37]; the results are summarized in Table 3. Our results obtained for both structures of SrS are in very good agreement with the experimental and earlier theoretical data. The structural phase stability and pressure-induced transitions from the B1 to the B2 structure are studied by performing the enthalpy ($H = E + PV$) calculations. Variation of enthalpy with pressure is shown in Fig. 7 for the two phases, which clearly shows that SrS transforms from the B1 to the B2 phase at 18.77 GPa. The transition pressures P_t predicted by our calculation is in good agreement with the experimental data and other theoretical calculations listed in Table 3.

5. CONCLUSIONS

In this paper, calculations of isotropic and directional Compton profiles, the electronic band structure, the density of states together with the lattice constant

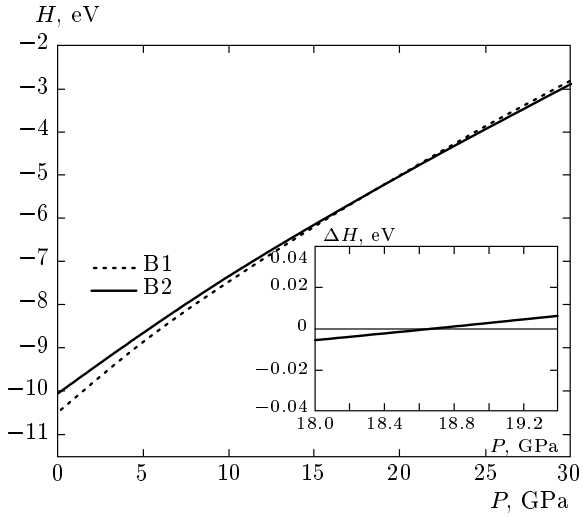

Fig. 7. Enthalpy calculated from the DFT-LCAO method for B1 and B2 structures of SrS. The inset shows the difference between the two data

and bulk modulus of SrS are reported using the *ab initio* LCAO method. The computed anisotropies, especially related to the [100] direction, very well reflect directional features of the momentum density distribution. The spherically averaged Compton profile is in good agreement with the first-ever measurement on SrS. The simple ionic calculation, which suggests transfer of 2.0 electrons from the valence s state of Sr to the p state of the S atom, shows poor agreement with experiment compared with the DFT-LCAO scheme. On the basis of EVED profiles, it is found that the bonding in SrS is less ionic or more covalent than in SrO. The first-principle total energy calculations for the B1 and B2 phases are performed to compute the lattice constant and the bulk modulus. The results are in very good agreement with earlier investigations and suggest the structural phase transition from B1 to B2 at 18.77 GPa.

This work is financially supported by the University Grant Commission (UGC) through Emeritus Fellowship and SR/33-37/2007 to BKS and SR/39-982/2010 to GS. GS is also thankful to the Head, Department of Pure & Applied Physics, University of Kota, Kota for providing the computational facilities.

REFERENCES

1. K. Syassen, Phys. Stat. Sol. A **91**, 11 (1985).
2. M. Souadika, B. Bennecer, F. Kalarasse, and A. Mellouki, Comput. Mater. Sci. **50**, 1701 (2011).
3. S. Ugur, Mater. Sci. Eng. B **162**, 116 (2009).
4. L. Y. Lu, J. J. Tan, O. U. Jia, and X. R. Chen, Physica B **399**, 66 (2007).
5. R. Khenata, H. Baltache, M. Rerat et al., Physica B **339**, 208 (2003).
6. I. B. Shameen Banu, M. Rajagopalan, B. Planivel, G. Kalpana, and P. Shenbagaraman, J. Low Temp. Phys. **112**, 211 (1998).
7. D. Varshney, N. Kaurav, R. Kinge, and R. K. Singh, Comput. Mater Sci. **41**, 529 (2008).
8. Y. Kaneko and T. Koda, J. Crystal Growth **86**, 72 (1988).
9. S. Labidi, M. Labidi, H. Meradji, S. Ghemid, and F. El Haj Hassan, Comp. Mat. Sci. **50**, 1077 (2011).
10. A. Shaukat, Y. Saeed, S. Nazir, N. Ikram, and M. Tanveer, Physica B **404**, 3964 (2009).
11. S. Zhang, H. Li, H. Li, S. Zhou, and X. Cao, J. Phys. Chem. B **111**, 1304 (2007).
12. Z. Charifi, H. Baaziz, F. El Haj Hassan, and N. Bouarissa, J. Phys.: Condens. Matter **17**, 4083 (2005).
13. D. Rached, M. Rabah, N. Benkhettou, B. Soudini, and H. Abid, Phys. Stat. Sol. B **241**, 2529 (2004).
14. W. Y. Ching, F. Gan, and M. Z. Huang, Phys. Rev. B **52**, 1596 (1995).
15. R. Pandey, J. E. Jaffe, and A. B. Kunz, Phys. Rev. B **43**, 9228 (1991).
16. V. S. Stepanyuk, A. Szasz, O. V. Farberovich et al., Phys. Stat. Sol. B **155**, 215 (1989).
17. M. J. Cooper, Rep. Prog. Phys. **48**, 415 (1985); B. Williams, *Compton Scattering*, McGraw-Hill, New York (1977), p. 13.
18. M. J. Cooper, P. E. Mijnarends, N. Shiotani, N. Sakai, and A. Bansil, *X-ray Compton Scattering*, Oxford Univ. Press, New York (2004), p. 8.
19. B. K. Sharma, A. Gupta, H. Singh et al., Phys. Rev. B **37**, 6821 (1988).
20. D. N. Timms, *Compton-Scattering Studies of Spin and Momentum Densities*, Ph. D. Thesis, University of Warwick (1989).
21. J. Felsteiner, P. Pattison, and M. J. Cooper, Phil. Mag. **30**, 537 (1974).

22. F. Biggs, L. B. Mandelsohn, and J. B. Mann, At. Data Nucl. Data Table **16**, 201 (1975).

23. R. Dovesi, V. R. Saunders, C. Roetti et al., CRYSTAL06 User's manual, University of Torino, Torino (2006).

24. http://www.tcm.phy.cam.ac.uk/.

25. J. P. Perdew, K. Burke, and M. Ernzerhof, Phys. Rev. Lett. **77**, 3865 (1996).

26. M. S. Dhaka, G. Sharma, M. C. Mishra et al., Compt. Phys. Commun. **182**, 2017 (2011).

27. M. C. Mishra, G. Sharma, R. K. Kothari, Y. K. Vijay, and B. K. Sharma, Comput. Mater. Sci. **51**, 340 (2012).

28. N. Munjal, G. Sharma, V. Vyas, K. B. Joshi, and B. K. Sharma, Phil. Mag. **92**, 3101 (2012).

29. A. D. Becke, J. Chem. Phys. **98**, 5648 (1993).

30. G. Sharma, M. Sharma, M. C. Mishra et al., Phys. Stat. Sol. B **246**, 2263 (2009).

31. V. Vyas, R. Kumar, M. C. Mishra, G. Sharma, and B. K. Sharma, Phys. Scr. **84**, 025601 (2011).

32. M. S. Dhaka, U. Paliwal, G. Sharma et al., J. Alloys Comp. **501**, 136 (2010).

33. W. A. Reed and P. Eisenberger, Phys. Rev. B **6**, 4596 (1972).

34. G. Sharma, K. B. Joshi, M. C. Mishra et al., J. Alloys Comp. **485**, 682 (2009).

35. R. Kumar, N. Munjal, G. Sharma et al., Phase Transition **85**, 1098 (2012).

36. J. C. Phillips, Rev. Mod. Phys. **42**, 317 (1970).

37. F. Birch, Phys. Rev. B **71**, 809 (1947); F. D. Murnaghan, Proc. Nat. Acad. Sci. USA **30**, 244 (1944).